Interactive Cloud Formation and Climatic Temperature Perturbations

KUO-NAN LIOU, S. C. S. OU AND P. J. LU

Department of Meteorology, University of Utah, Salt Lake City, UT 84112

(Manuscript received 12 October 1984; in final form 26 February 1985)

ABSTRACT

A one-dimensional climate model with an interactive cloud formation program is developed to investigate its effects on temperature perturbations due to various radiative forcings including doubling of CO_2, a 2% increase of the solar constant and the increase of the cirrus IR emissivity. By virtue of the *K*-theory for turbulence transfer of sensible and latent heat fluxes, we demonstrate that the model may be described by a set of partial differential equations governing the thermodynamic energy balance, water vapor transport, vertical velocity in the cloudy region and cloud cover. In particular, we illustrate that the climatic temperature perturbation experiment may be carried out as a boundary value problem. Moreover, in order to effectively incorporate interactive cloud formation and radiative transfer programs in the model, we have designed a cloud compaction scheme based on statistical and stochastic procedures for the estimate of cloud covers, thicknesses, heights and positions for high, middle and low clouds. We show that, overall, the interactive cloud formation program reduces the sensitivity of temperature increases caused by positive radiative forcings and therefore generates a negative feedback in reference to the fixed cloud program. Low and high cloud formations lead to negative feedbacks as a result of the increased low cloud cover and thickness and decreased high cloud cover and thickness caused by temperature increases. The former strengthens the solar albedo effects, whereas the latter weakens the IR greenhouse effects. On the other hand, the middle cloud formation exhibits a positive feedback because of the reduction in cloud cover and thickness. Further, we show that the cloud cover variation alone will produce a larger reduction in temperature increases. In light of these experimental results, it appears physically appropriate to conclude that an interactive cloud formation program with radiative transfer coupling in the context of a model setting will lead to a negative feedback in temperature sensitivity analyses.

1. Introduction

It has been recognized physically that proper understanding of cloud–radiation interactions and feedback within the earth–atmosphere system holds the key to success for the solution of the earth's climate and climatic perturbations due to various internal and external radiative forcings. Amid difficulties in the definition of clouds within a numerical model setting, it is quite apparent that clouds exert two competitive effects on the radiation field of the earth and the atmosphere. On one hand, clouds reflect a significant portion of the incoming solar flux, and on the other, clouds also trap the outgoing thermal infrared fluxes emitted from the surface and the atmosphere below them. The competition of the solar albedo and IR greenhouse effects determines whether the earth–atmosphere system will undergo cooling or warming. Within the atmosphere and at the surface, other thermodynamic and dynamic factors will also modify the atmospheric thermal structure on the local scale. Interaction between cloud-radiation and dynamic processes is clearly the most important physical coupling in weather and climate systems.

Essentially all one-dimensional radiative–convective or radiative–turbulent models either prescribe the cloud cover, thickness and height or assume the cloud position according to the temperature specification in radiative forcing experiments (e.g., see Manabe and Wetherald, 1967; Ramanathan and Coakley, 1978; Hansen *et al.*, 1981; Liou and Ou, 1983, etc.). The only exception is the work presented by Hummel and Kuhn (1981). In their pioneering analysis, the water vapor transport and cloud formation are interactive based on a fixed cloud-cover value. Layered cloud analyses with respect to the transfer of solar and IR fluxes were not given, nor were the detailed mathematical and physical fundamentals presented in the paper, however.

On the cloud formation side, Sasamori (1975) proposed an interesting one-dimensional cloud model for the computation of fractional cloudiness, liquid water content and rate of precipitation. More recently, Sundqvist (1978) developed a cloud generation model for nonconvective condensation processes based on parameterizations of evaporation and precipitation terms. In this paper, we wish to develop a cloud formation scheme in the context of a one-dimensional space and in harmony with the thermodynamic equilibrium climate model proposed by Liou and Ou (1983). The prime objective of this development is to construct a one-dimensional climate model composed of an interactive cloud formation and radiative transfer computational program by virtue of the fundamental

physical analyses and appropriate mathematical definitions. In addition, we wish to investigate the effects of, and to derive physical insight into, cloud–radiation interactions and feedback on the climatic temperature perturbations due to various radiative forcings. Section 2 describes the development of the basic thermodynamic model with a number of physical postulations and assumptions imposed. The cloud compaction scheme for the formation of high, middle and low cloud types is presented in Section 3. In Section 4, we demonstrate that the climatic perturbation experiments may be carried out as boundary value problems. Results of the numerical experiments are presented in Section 5. Finally, concluding remarks are given in Section 6.

2. One-dimensional climate model with interactive cloud formation program

In the context of a one-dimensional space, the thermodynamic energy equation may be written in the form

$$\frac{\partial}{\partial t}\rho\,(C_pT + Lq) = \frac{\partial}{\partial z}(F_S - F_{IR}) - \frac{\partial}{\partial z}F_v, \quad (2.1)$$

where ρ denotes the density of air, C_p the specific heat at constant pressure, T the temperature, and F_S, F_{IR} and F_v represent the net solar, thermal infrared and vertical fluxes. We consider steady-state conditions so that $\partial T/\partial t = \partial q/\partial t = 0$ and then integrate Eq. (2.1) over the atmospheric column from z to ∞ to obtain

$$[F_S(\infty) - F_{IR}(\infty)] - [F_S(z) - F_{IR}(z)] = F_v(\infty) - F_v(z). \quad (2.2)$$

The boundary conditions for the aforementioned first-order differential equation are that $F_S(\infty) = F_{IR}(\infty)$ and that $F_v(\infty) = 0$. These conditions imply that the vertical eddy flux goes to zero at the top of the atmosphere where the net solar flux must be balanced by the IR flux under equilibrium conditions. Thus, we find

$$F_v(z) + F_{IR}(z) = F_S(z). \quad (2.3)$$

The vertical eddy fluxes of sensible and latent heat are given by $\overline{\rho w'(C_pT' + gz' + Lq')}$, where w is the vertical velocity. On using the K-theory for the eddy fluxes and incorporating a counter gradient factor γ' for the eddy sensible heat flux (Deardorff, 1972), Eq. (2.3) may be expressed in terms of temperature and humidity variables in the form

$$-k_z\rho C_p\left(\frac{\partial T}{\partial z} + \gamma_d - \gamma'\right) - k'_z\rho L\frac{\partial q}{\partial z} + \int_0^\infty \sigma T^4(z')K(|z - z'|)dz' = F_S(z), \quad (2.4)$$

where k_z and k'_z denote the thermal and water vapor eddy diffusion coefficients, respectively, γ_d the adiabatic lapse rate, q the specific humidity, and L the latent heat of vaporization and condensation. In addition, we have expressed the net IR flux in terms of the temperature to the fourth power and the broadband emissivity kernel K (Liou and Ou, 1983).

In order to introduce an interactive humidity program from which cloud fields may be formed, we require an additional equation to specify the specific humidity q. Here we also note that the humidity field will affect the IR emissivity kernel and solar net flux depicted in Eq. (2.4).

In line with the one-dimensional equilibrium model defined previously, we may postulate physically that the variation of the eddy flux of water vapor in the vertical may be balanced by the sinks and sources, due to condensation and evaporation, respectively, of water vapor molecules. Therefore, when the K-theory for the eddy flux of water vapor is introduced we may write

$$\frac{\partial}{\partial z}\overline{\rho w'q'} = -\frac{\partial}{\partial z}\left(k'_z\rho\frac{\partial q}{\partial z}\right) = \eta Q_c/L - (1 - \eta)E_r/L, \quad (2.5)$$

where η represents the cloud cover formed by the condensation process, and Q_c and E_r denote, respectively, the heating rates produced by condensation and evaporation. It is evident that in order to compute the transport of water vapor, three additional variables have been introduced, namely, cloud cover η, condensational heating Q_c, and evaporation heating E_r. Sundqvist (1978) has developed a comprehensive parameterization equation for the computation of the evaporation term that is related to the integrated precipitation rate. The precipitation rate is further related to the cloud liquid water content. Thus, three additional equations are needed to close the system and the computations for the equilibrium temperature and humidity become extremely complicated. Since the prime objective of this investigation is to physically understand the effects of an interactive cloud formation program on climatic temperature perturbations, we shall assume that the evaporation term is much smaller than the condensation term. This, in effect, assumes that all the condensates fall immediately as precipitation without reevaporation; an assumption which has been widely used in numerical modeling for weather and climate processes.

In order to get an analytic expression for the condensational heating Q_c, let us assume that in the cloudy region the vertical velocity is w_s. The vertical flux of saturation specific humidity q_s is then given by $\rho w_s q_s$. Note that the vertical velocity w_s so defined is associated with diabatic heating including latent, radiative and sensible heat exchanges. Moreover, on the basis of the energy conservation principle the condensational heating Q_c must be a result of the divergence of $\rho w_s q_s L$. Subject to these conditions, Eq. (2.5) may be rewritten in the form

$$-\frac{\partial}{\partial z}\left(\rho L k_z' \frac{\partial q}{\partial z}\right) = \eta L \frac{\partial}{\partial z}(\rho w_s q_s). \quad (2.6)$$

Here, we have introduced a new unknown variable, w_s, so as to compute q.

Now, we need one additional equation to evaluate the vertical velocity in the cloudy region. For this purpose, we modify the Richardson's equation (see Dutton, 1976, p. 188) for the one-dimensional space in the form

$$Q_c/\rho = C_p \frac{dT}{dt} - \alpha \frac{dp}{dt} = C_p w_c\left(\frac{dT}{dz} + \gamma_d\right). \quad (2.7)$$

We have used the hydrostatic equation to get the last form, where $w_c = dz/dt$ is the vertical velocity associated with condensation processes only. From general circulation statistics (e.g., see Oort and Rasmusson, 1971), the globally averaged mean vertical velocity is $\bar{w} \approx 0$. Let the vertical velocity in the cloudy and clear regions be denoted by w_s and w_0, respectively. Also, let the vertical velocity associated with condensation processes be w_c. Since the forcing in the cloudy region may be considered as a combination of sensible and radiative flux exchanges in the clear portion and condensation, then by virtue of the thermodynamic equation denoted in Eq. (2.7), we may write $w_s \approx w_0 + w_c$. Moreover, since the globally averaged mass balance requires $\bar{w} = \eta w_s + (1 - \eta)w_0 = 0$, we must have $w_s = (1 - \eta)w_c$. It follows that Eqs. (2.6) and (2.7) may be combined to give

$$L \frac{\partial}{\partial z}(\rho w_s q_s) = \frac{\rho C_p}{1 - \eta} w_s\left(\frac{dT}{dz} + \gamma_d\right). \quad (2.8)$$

To close the system, we need one more equation to compute η. Let the relative humidity for a clear column be h_0, then the area-averaged relative humidity may be expressed by

$$h = \frac{q}{q_s(T)} = (1 - \eta)h_0 + \eta h_c, \quad (2.9)$$

where the relative humidity for the cloud portion h_c is taken to be unity. The relative humidity for the clear column h_0 is referred to as the "threshold relative humidity", which needs to be parameterized. In the present study, the threshold relative humidity is taken to be a function of height as suggested by Manabe and Wetherald (1967) in the form

$$h_0 = h_{0s}(P/P_s - 0.02)/0.98, \quad (2.10)$$

where h_{0s} is the threshold relative humidity at the surface, P is the pressure, and P_s the surface pressure. This relative humidity profile was originally used for the averaged cloudy sky conditions. However, we find that Manabe and Wetherald's profile is steeper than the climatological humidity profile depicted in Fig. 1. Thus, by using their profile for the clear sky, the averaged cloudy sky relative humidity will be closer to climatological values. It is noted that the only prescribed value is the threshold relative humidity at the surface, which is considered to always be clear in the model; i.e., cloud formation in the lowermost layer is not allowed. Sensitivity of the cloud formation model to the prescribed threshold relative humidity at the surface will be discussed in the results section.

Having h_0 fixed, Eq. (2.9) may then be written in the form

$$\eta = \left[\frac{q}{q_s(T)} - h_0\right]\Big/(1 - h_0). \quad (2.11)$$

By virtue of this relationship, once the temperature

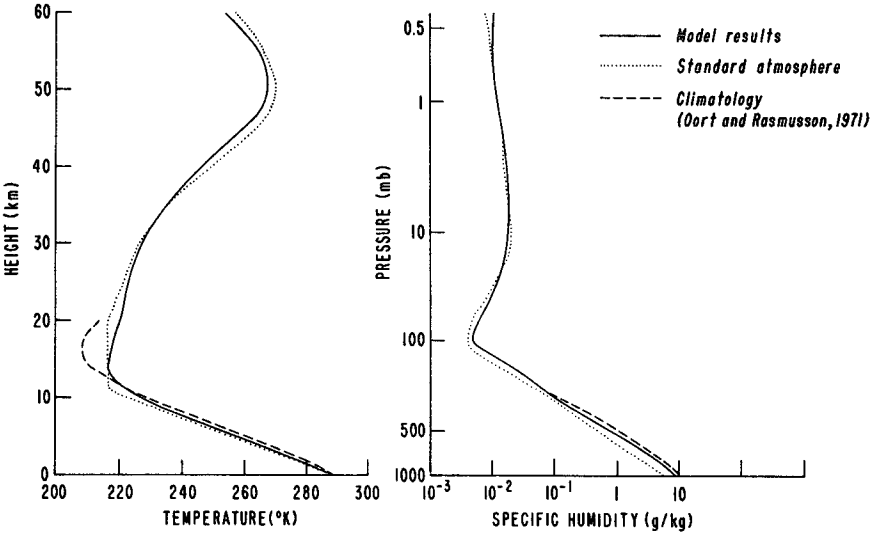

FIG. 1. Temperature and specific humidity profiles computed from the present model under standard atmospheric conditions. Comparisons are made with those corresponding to a standard atmosphere and climatological data compiled by Oort and Rasmusson.

and humidity fields have been derived from Eqs. (2.4) and (2.6), cloud covers on some specified vertical layers may then be computed from Eq. (2.14). In Sundqvist's pioneering cloud formation work, h_0 is assumed to be 0.8. We also note that in the formation of large-scale cloud fields in general circulation models for medium range weather prediction, the critical relative humidity h_c, which is equivalent to h_0 defined here, is taken to be a nonlinear function of pressure (Geleyn, 1981; Liou and Zheng, 1984). As shown, Eqs. (2.4), (2.6), (2.8) and (2.11) represent a closed system of differential equations for simultaneous computations of T, q, w_s and η. Two profiles of the eddy transport coefficients k_z and k'_z, however, need to be specified in order to solve these four variables as functions of height.

To get k_z and k'_z, we first begin with the determination of the surface fluxes of sensible and latent heat. Following the parameterization scheme proposed by Ou and Liou (1984) who utilized Budyko's (1982) climatological data in the statistical analysis, the total surface sensible and latent heat flux may be expressed by the following nonlinear equation:

$$H = \overline{\rho C_p w'T' + \rho L w'q'}|_{z\to 0} = C_1\left[\left|\frac{\partial T}{\partial z}\right| + \frac{L}{C_p}\left|\frac{\partial q}{\partial z}\right|\right]_{z\to 0}^{C_2}, \tag{2.12}$$

where the empirical-statistical coefficients C_1 and C_2 have values of 37 and 0.276, respectively, when H is in units of W m^{-2}. To separate the sensible and latent heat fluxes, we make use of the concept of the Bowen ratio defined by

$$B = \frac{\text{sensible heat flux}}{\text{latent heat flux}} = \frac{H_S}{H_L}, \tag{2.13}$$

where $H_S + H_L = H$. According to Budyko's analysis, $B \approx 0.193$ for the mean annual condition. It follows that the eddy thermal and water vapor diffusion coefficients at the surface may be computed by

$$k_z|_{z\to 0} = -H_S \Big/ \left(\rho C_p \frac{\partial T}{\partial z}\right)_{z\to 0}, \tag{2.14}$$

$$k'_z|_{z\to 0} = -H_L \Big/ \left(\rho L \frac{\partial q}{\partial z}\right)_{z\to 0}. \tag{2.15}$$

In the troposphere, we make use of the mixing length theory proposed by Liou and Ou (1983) for the computation of the thermal eddy diffusion coefficients. While we recognize the simplicity of the mixing length model in turbulent atmospheres, we postulate that

$$k_z \propto \overline{l^2}\left|\frac{\partial \bar{u}}{\partial z}\right|. \tag{2.16}$$

Furthermore, the mean wind shear, in the limit of one-dimensional models, may be approximated by a linear equation in height such that $\partial\bar{u}/\partial z = az + b$, with a and b denoting empirical coefficients. Now, we need an additional upper boundary condition to determine these two coefficients. For this purpose, we employ the eddy thermal diffusion coefficient value at the tropopause given by Reed and German (1965). Thus, with k_z values known at the surface and tropopause, coefficients a and b can be computed. Since the water vapor eddy diffusion coefficient k'_z is less known and since adequate and reliable k'_z data at the tropopause are not available, we have assumed that the profile of k'_z has the same shape as that of k_z.

3. Cloud compaction scheme

Once the clouds are formed in the model layers, it is necessary to perform appropriate averages so that high, middle and low clouds are defined in terms of their fractional coverages and thicknesses. This is in view of the fact that the present one-dimensional model is structured with a high vertical resolution with respect to the cloud forming layers. We will discuss the requirement of the vertical layer with respect to the formation of high, middle and low clouds as we proceed with the cloud analysis. First, let us assume that M upper layers are classified as high cloud layers and that in the ith layer the model generates η_i fractional cover with top and base heights given by z_{ti} and z_{bi}, respectively. Also, let $z_{mi} = (z_{ti} + z_{bi})/2$ which denotes the midpoint of the layer. Next, we perform ensemble averages in the forms

$$\eta^{(1)} = \frac{1}{M}\sum_{i=1}^{M}\eta_i, \tag{3.1a}$$

$$z_m{}^{(1)} = \frac{1}{M}\sum_{i=1}^{M}\eta_i z_{mi}. \tag{3.1b}$$

We then compute the high cloud top and base heights utilizing the following schemes:

$$z_b{}^{(1)} = z_{b1} + [1 - \eta^{(1)}][z_m{}^{(1)} - z_{b1}], \tag{3.2a}$$

$$z_t{}^{(1)} = z_{tM} - [1 - \eta^{(1)}][z_{tM} - z_m{}^{(1)}]. \tag{3.2b}$$

The cloud thickness is therefore given by $\Delta z^{(1)} = z_t{}^{(1)} - z_b{}^{(1)}$. These equations take into consideration the limits of clear and overcast conditions; when $\eta = 0$, $z_b{}^{(1)} = z_m{}^{(1)} = z_t{}^{(1)}$; i.e., $\Delta z^{(1)} = 0$. On the other hand, when $\eta = 1$, (i.e., all sublayers are completely covered by clouds) $\Delta z^{(1)} = z_{tM} - z_{b1}$, where we note that z_{b1} and z_{tM} denote the base height for the lower most layer and the top height for the upper most layer, respectively. Similarly, we may apply the procedures of these ensemble averages to middle and low cloud layers to obtain $[\eta^{(2)}, \Delta z^{(2)}]$ and $[\eta^{(3)}, \Delta z^{(3)}]$. After numerous experimentations, the minimum vertical layers required to converge the cloud covers and thicknesses are found to be about 12. Also, in line with the standard profile, we use the temperature criteria of -20, 2 and 10°C

for the base heights of high, middle and low clouds, respectively.

At this point, we require available climatological data for the cloud cover and thickness to verify the model cloud scheme. Fortunately or unfortunately, the only sources of available cloud data have been those provided by London (1957). London classified clouds into six types and tabulated the fraction of cloud cover, cloud top and base heights for 10 latitudinal belts. Based on his cloud data, we carry out area averages to obtain northern hemispheric values listed in Table 1.

The next step would be to compact these six cloud types into high, middle and low clouds in line with model calculations. For this purpose, we assign cumulus and stratus to be low clouds, and consider nimbostratus and cumulonimbus to be a combination of middle and low clouds. The latter consideration is based on the climatological base and top heights of Ns and Cb provided by London. Accordingly, the observed cloud cover and top and base heights may be calculated from

$$\eta_*^{(1)} = \eta(\mathrm{Ci}), \tag{3.3a}$$

$$\eta_*^{(2)} = \eta(\mathrm{As}) + \eta(\mathrm{Ns}) + \eta(\mathrm{Cb}), \tag{3.3b}$$

$$\eta_*^{(3)} = \eta(\mathrm{Cu}) + \eta(\mathrm{St}) + \eta(\mathrm{Ns}) + \eta(\mathrm{Cb}), \tag{3.3c}$$

where values with subscript $*$ denote climatological data. Moreover, thicknesses for As and Ci are assigned to be those for middle and high clouds, respectively, while the thickness for the low cloud is assumed to be the average of those for Cu and St. Thus, the three cloud thicknesses are

$$\Delta z_*^{(1)} = \Delta z(\mathrm{Ci}), \tag{3.4a}$$

$$\Delta z_*^{(2)} = \Delta z(\mathrm{As}), \tag{3.4b}$$

$$\Delta z_*^{(3)} = [\Delta z(\mathrm{Cu}) + \Delta z(\mathrm{St})]/2. \tag{3.4c}$$

At this point, we have generated high, middle and low clouds in the model whose cloud cover and thickness values could be verified with observed climatological data. However, for radiative transfer calculations, information on the physical position of clouds is needed. If the fractions of high, middle and low clouds are less than one then, in principle, there would be infinite possible configurations for these clouds in a certain grid region. The most straightforward means to treat the overlap problem is to assume that the total cloud cover is equal to the maximum cloud cover corresponding to one of the three cloud types. However, in view of the fact that there are certain stochastic processes governing the formation and maintenance of water droplets and ice crystals in the atmosphere, it appears physically appropriate to utilize statistics to evaluate the total cloud cover within a defined scene. This approach appears most appropriate for the one-dimensional climate model. Hence, we shall postulate that the overlap of high, middle and low clouds is in a random fashion statistically so that the total cloud cover is given by

$$\eta^{(t)} = 1 - [1 - \eta^{(1)}][1 - \eta^{(2)}][1 - \eta^{(3)}]. \tag{3.5}$$

Furthermore, since the total cloud cover value $\eta_*^{(t)}$ is available from observed data (see Table 1), we may apply a correction factor uniformly to each cloud type such that

$$\eta_*^{(t)} = 1 - [1 - \eta^{(1)}a][1 - \eta^{(2)}a][1 - \eta^{(3)}a], \tag{3.6}$$

where a is a weighting constant that can be computed from Eq. (3.6). We then let $\eta_a{}^{(1)} = \eta^{(1)}a$, $\eta_a{}^{(2)} = \eta^{(1)}a$ and $\eta_a{}^{(3)} = \eta^{(3)}a$. These values are assumed to be the correct cloud covers for high, middle and low clouds. Finally, vertical liquid water contents for various cloud types may be calculated utilizing the observed particle size distributions (see Liou and Zheng, 1984). Since the cloud cover, thickness, position and liquid water content are now known, computations of the transfer of solar and IR radiative fluxes in cloudy atmospheres subject to the plane-parallel approximation may be carried out.

4. Climate perturbation experiments as boundary value problems

Summarizing the discussion given in Section 2 and having the cloud parameters defined, the climate system involving radiative processes, turbulent transfer and cloud formation in the context of one-dimensional space may be described by the following system of equations:

$$a(z)\frac{\partial T}{\partial z} + b(z)\frac{\partial q}{\partial z} + \int_0^\infty \sigma T^4(z')K(|z - z'|)dz' = c(z), \tag{4.1}$$

TABLE 1. Cloud type, cloud cover and thickness for the Northern Hemisphere.

Cloud type	Cu	Middle (As)	High (Ci)	Ns	Cb	St	Total
Cloud cover	0.116	0.074	0.156	0.081	0.033	0.120	0.511
Cloud top (km)	2.52	4.26	10.94	3.56	3.20	1.45	—
Cloud base (km)	1.70	3.50	9.24	1.35	1.70	1.35	—

$$\frac{\partial}{\partial z}\left(b(z)\frac{\partial q}{\partial z}\right) = \eta\frac{\partial f}{\partial z}, \tag{4.2}$$

$$(1-\eta)\frac{\partial \ln f}{\partial z} = \frac{C_p}{L}\frac{1}{q_s}\left(\frac{\partial T}{\partial z} + \gamma_d\right), \tag{4.3}$$

$$\eta = \left(\frac{q}{q_s} - h_0\right)\Big/(1-h_0), \tag{4.4}$$

where

$$a(z) = -\rho C_p k_z, \tag{4.5}$$

$$b(z) = -\rho L k'_z, \tag{4.6}$$

$$c(z) = F_s(z) + \rho C_p k_z(\gamma_d - \gamma'), \tag{4.7}$$

$$f(z) = \rho L w_s(z) q_s[T(z)]. \tag{4.8}$$

Here we note that $f(z)$ represents the vertical saturation latent heat flux in the cloudy region. Equations (4.1)–(4.4) contain four unknown variables, namely, temperature T, specific humidity q, vertical velocity in the cloudy region w_s in terms of the vertical latent heat flux, and cloud cover η. These four variables are functions of height z and are to be solved simultaneously subject to the required physical boundary conditions.

Equation (4.1) is a first-order partial differential equation in T. Its required boundary condition is that net eddy heat and radiative fluxes must be balanced at the surface under equilibrium conditions. It follows that

$$H + \sigma T_0^4 - F^{\downarrow}_{\mathrm{IR}}(0) = F_S(0), \tag{4.9}$$

where T_0 is the surface temperature, $F^{\downarrow}_{\mathrm{IR}}$ the downward IR flux reaching the surface and the upward surface heat flux H has been given in Eq. (2.15). Further, Eq. (4.2) is a second-order partial differential equation in q which requires two boundary conditions for the solution of the equation. At the surface the cloud cover $\eta = 0$ so that

$$q(0) = q_s(T_0)h_0, \tag{4.10}$$

where h_0 is the threshold relative humidity defined in Eq. (2.10). In addition, at the level of the tropopause z_*, we impose the condition that no cloud is allowed to form. This leads to

$$q(z_*) = q_s(T_*)h_0. \tag{4.11}$$

Finally, we need one additional boundary condition for the solution of f. On the basis of the mass conservation principle and in reference to Eq. (2.15), the divergence of the vertical flux of saturation specific humidity in the cloudy region must be balanced by the surface evaporation flux. Thus,

$$H_L = -\int_{z_b}^{z_t} \eta\frac{\partial f}{\partial z}\,dz. \tag{4.12}$$

Having the boundary conditions explicitly defined, Eqs. (4.1)–(4.4) may now be solved numerically. Detailed finite-difference solutions to these equations are given in the Appendix.

5. Results and discussion

To carry out numerical experiments to simulate the present mean annual condition, the following input data were used: the solar constant S, average cosine of the solar zenith angle μ_0, duration of sunlight, surface albedo, and CO_2 concentration are taken to be 1360 W m^{-2}, 0.5, 12 h, 0.13, and 330 ppmv, respectively. The ozone and molecular profiles employed are those corresponding to the standard atmospheric condition. In addition, all clouds, except cirrus, are assumed to be black. The mean cirrus IR emissivity is set to be 0.47 according to the analysis given by Ou and Liou (1984). Solar reflection (albedo) and transmission values for cirrus are related to the IR emissivity via the vertical ice content.

Figure 1 illustrates temperature and specific humidity profiles computed from the present model. In this figure, comparisons are also made with those corresponding to the standard atmospheric condition and those compiled by Oort and Rasmusson (1971) whose data are available only up to about 20 km. The simulated temperature profile with the input parameters noted above agrees closely with that of the standard atmosphere. It also matches with that provided by Oort and Rasmusson in the troposphere. With respect to the humidity profile, the present results are in general agreement with those given by Oort and Rasmusson, but are greater than those of the standard atmospheric condition. The agreement between computed values and observed data, however, is excellent in the stratosphere. As for the cloud parameters, the cloud cover, height and thickness computed from the scheme described in Section 3 and depicted in Fig. 2 are within about 10% of those analyzed from London's data. This good comparison is quite encouraging since model results and observed data were derived from separate statistical means.

In the present one-dimensional model, the cloud cover is calculated interactively and physically via the thermodynamic equation, the water vapor transport equation, the vertical saturation latent heat flux in the cloudy region and the cloud cover equation, all of which are derived from appropriate physical definitions stated in Section 4. Note, however, that a number of general circulation models designed for climate sensitivity studies utilize empirical–statistical methods for the calculation of the cloud cover. For instance, in Washington and Meehl (1984), the fractional cloud cover is assumed to be 95% for nonconvective clouds and 30% for convective clouds. In Wetherald and Manabe (1980), a cloud amount of 80% is assigned to condensation so that the model atmosphere will equil-

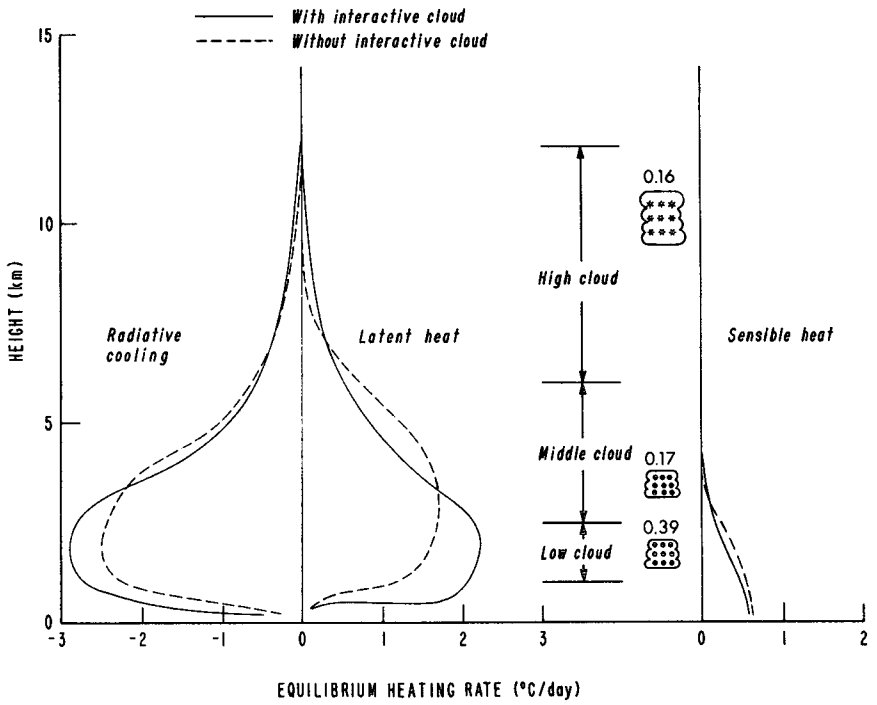

FIG. 2. Equilibrium heating rate profiles produced by the exchanges of radiative, latent and sensible heat fluxes with and without the incorporation of an interactive cloud formation program. Also depicted are the cloud covers, thicknesses and heights for high, middle and low clouds generated from the interactive cloud formation program.

ibrate at a realistic temperature by maintaining a realistic area mean cloud amount. In Hansen *et al.* (1983), the large-scale cloud formation is empirical without a specific physical and mathematical equation for cloud cover calculations. Moreover, the one-dimensional model has the advantage of high vertical resolution so that realistic high, middle and low clouds can be defined by the statistical and stochastic procedures illustrated in Section 3. Also, in the one-dimensional model, one can incorporate more sophisticated IR and solar radiation programs so that cloud–radiation interactions and feedbacks may be comprehensively investigated and physically understood, as demonstrated below. We must add that the one-dimensional cloud model developed here is based on a globally averaged condition without the consideration of horizontal advection and meridional transport, and therefore, it may not be appropriate to directly compare the present results with those derived from general circulation models.

In Section 2, we indicated that the threshold relative humidity h_{0s} is prescribed with a value of 85%, representing the climatological mean. We have performed sensitivity analyses on the variations of cloud cover due to the uncertainty of h_{0s} employing 80% and 90% in the cloud formation experiment. Table 2 summarizes the cloud cover results for high, middle and low cloud types without the statistical adjustments described in Eqs. (3.5) and (3.6). Increasing the surface relative humidity leads to a decrease of the cloud cover for all three cloud types. The prime reason for these decreases is the reduction of the relative humidity gradient near the surface which, in turn, reduces the surface evaporation flux according to Eq. (2.12). As shown in Table 2, the cloud cover values are relatively stable without abnormal changes due to the uncertainty of h_{0s}. In the control run and the subsequent sensitivity experiments involving various radiative forcings, h_{0s} is taken to be 85%.

Next, we present heating rate profiles produced by net radiative, latent and sensible heat flux exchanges under thermodynamic equilibrium conditions for cases with and without the incorporation of the interactive cloud program into the model. In the latter case, cloud covers and positions for high, middle and low clouds are prescribed according to equilibrium values. In reference to the heating rate due to the latent heat release

TABLE 2. Cloud cover results for high, middle and low cloud types using three values for the threshold relative humidity at the surface.

h_{0s}	90%	85%	80%
Low	0.384	0.389	0.392
Middle	0.162	0.175	0.184
High	0.152	0.159	0.164

in Fig. 2, it is seen that the interactive cloud program produces larger heating in the lower atmosphere as compared with the fixed cloud case. This is due to the fact that more condensation takes place in this region, which leads to a larger formation rate of low clouds. The coupled radiative cooling generated by infrared flux exchanges due to this larger cloud cover is also increased so that a thermodynamic balance can be achieved. The sensible heat is generally confined in the atmosphere below about 4 km and is about the same for both cases. Moreover, the total precipitation rate, assuming all condensates fall instantaneously, may be computed from the integration of the latent heat profile. The value that we obtained is about 107.1 cm/yr which compares favorably with the climatological data of 98.1 and 109.7 cm/yr provided by Sellers (1965) and Budyko (1982), respectively.

In order to understand the sensitivity of the cloud formation on temperature perturbations, we design two numerical experiments. In the first experiment (referred to as Exp. 1), the effects of high, middle and low cloud covers computed from the interactive cloud formation on temperature perturbations are isolated by prescribing the cloud reflection and transmission and cirrus emissivity regardless of the cloud thickness formed in the model. In the second experiment (referred to as Exp. 2), cloud radiative properties vary as functions of the cloud thickness. In this manner, we may examine separately whether variations of various cloud covers and thicknesses due to positive radiative forcings lead to positive or negative feedback.

In Fig. 3, we show the temperature sensitivity involving the cloud interactive program by a number of radiative forcings, doubling of CO_2, a 2% increase of the solar constant and the increase of the mean cirrus emissivity from 0.47 to 0.62. Sensitivity results due to the effects of cloud cover only are denoted by dashed lines, and to a combination of cloud cover and thickness, by dots. Also depicted for comparison are sensitivity results produced by prescribing cloud parameters in the model experiment. These are shown by solid lines.

In the fixed cloud case, doubling of CO_2 leads to warming and cooling below and above 16 km, respectively. The tropospheric warming is on the order of 2°C with a surface value of 2.3°C. Inclusion of an interactive cloud formation program (Exp. 1) reduces the sensitivity of temperature increase in the troposphere. This reduced sensitivity is due to the fact that increasing surface temperature will lead to additional upward water vapor fluxes near the surface. As a result, more clouds could be formed in low atmospheric layers. On the basis of the conservation principle of water vapor fluxes, the possibility of more low cloud formation will also lead to the reduction of high and middle cloud formations. In our interactive cloud–CO_2 experiments, the increase of the low cloud cover is about 1.5%, whereas the decrease of middle and high cloud covers

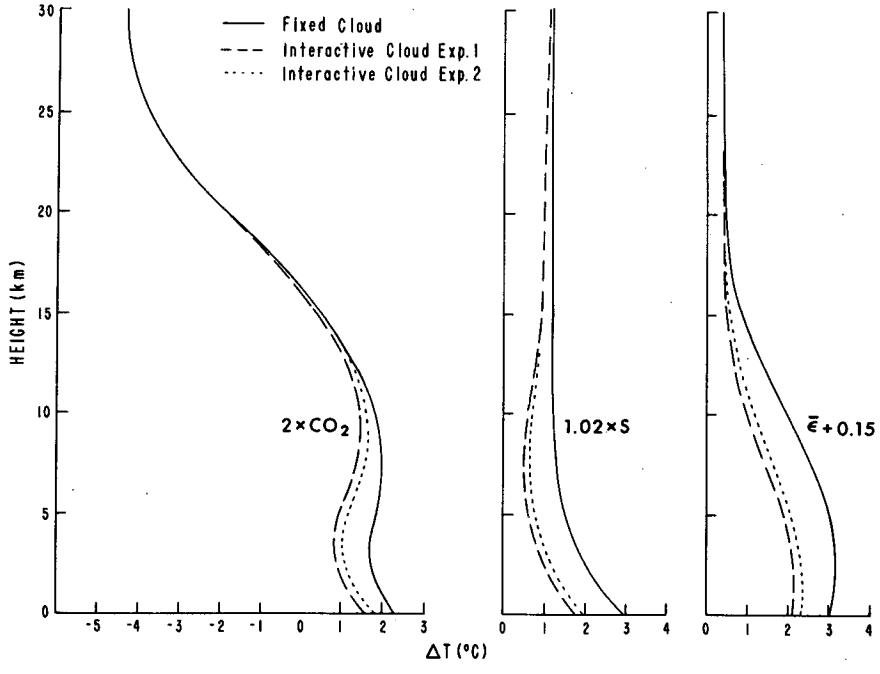

FIG. 3. Temperature increases in one-dimensional model settings due to doubling of CO_2, a 2% increase of the solar constant and the increase of the mean cirrus IR emissivity $\bar{\epsilon}$ by 0.15. Fixed cloud (solid lines), interactive cloud cover (dashed lines), interactive cloud cover and thickness (dots).

are, respectively, 3.2 and 2.0%. The consequence of these cloud cover variabilities is that increasing the low cloud cover leads to the prevalance of the solar albedo effect which will cause a negative feedback during the CO_2 greenhouse perturbation. In addition, decreasing the high cloud cover will reduce the IR greenhouse effect and therefore will also cause a negative feedback. But the decrease of middle cloud cover will lead to a positive feedback in the temperature perturbation. Overall, as indicated previously, the interactive cloud cover experiment produces a negative feedback in the sensitivity of temperature increase. Basically, these results are closely associated with the assumptions that low and middle clouds may be treated as black clouds and that high clouds are about half black. Also, the net negative feedback should be viewed in reference to the fixed cloud cover case. We note that Hummel and Kuhn (1981) also show a negative feedback in their one-dimensional cloud experiment. In addition, it is noted that the increase of the low cloud cover derived from the present study appears to be in general agreement with that concluded by Wetherald and Manabe (1980) in their general circulation experiments. In their GCM analyses, it was also pointed out that low cloud formation may be reduced in localized regions such as the middle latitudes and tropical rainbelts, as a result of horizontal advection, meridional transport, etc. Thus, it should be pointed out that the present results derived from a globally averaged condition may not be directly applicable to a three-dimensional model setting.

With respect to the 2% increase for the solar constant, the decrease of temperature sensitivity due to the insertion of an interactive cloud program is quite evident, especially in the lower atmosphere. At the surface, $\Delta T_s = 2.9°C$ for the fixed cloud case, but it is reduced to 1.7°C for the interactive cloud case. The increase of low cloud formation coupled with the decrease of middle and high clouds caused by the solar constant increase generates a negative response to the temperature perturbation. Finally, we perform sensitivity experiments involving the cirrus IR sensitivity. The cirrus IR emissivity of 0.47 used for the mean annual condition is replaced by 0.62. Increasing the cirrus emissivity values to less than about 0.9 (Ou and Liou, 1984) produces warming due to the enhanced greenhouse effect. The role of the interactive cloud program in Exp. 1 again is a negative feedback in the temperature perturbation. As is known in the field of atmospheric radiation, the cirrus IR emissivity is poorly understood both from observational and theoretical viewpoints. We have illustrated here that realistic variations of the cirrus emissivity could cause temperature perturbations on the same order of magnitude as those produced by a doubling of CO_2 and a 2% increase of the solar constant. Thus, it is of paramount importance to have adequate climatological data for the cirrus emissivity in conjunction with climate modeling efforts.

In Exp. 2, solar radiative properties of high, middle and low clouds and the IR emissivity of high clouds are allowed to change as a reflection of cloud thickness variations. In the interactive cloud formation program, not only cloud covers change, but also cloud thicknesses vary to a certain degree due to positive radiative forcings described above. We find that the low and middle cloud thickness increases and decreases, leading to enhanced and reduced solar albedo effects, respectively. Furthermore, high clouds become thinner, which will also lead to a smaller IR emissivity, and since solar reflection and transmission values do not change appreciably, the net radiative effect is the same as that of low clouds. Thus, the sign of feedback due to variations in cloud thicknesses is in line with cloud cover changes. However, the degree of influence differs somewhat. Overall, we find a positive feedback from Exp. 2 in reference to Exp. 1 as illustrated in Fig. 3. This is owing to the fact that the thickness Δz_m of the middle cloud reduces quite significantly in the aforementioned three experiments. In the doubling of CO_2 case, we find Δz_m is decreased by about 0.1 km resulting in solar reflection decreases from 0.65 to 0.61. On the other hand, the low cloud thickness is decreased by only 0.02 km and this decrease does not produce significant changes in solar reflection. High clouds also become thinner and therefore exert a negative feedback response caused by a slight decrease of the IR emissivity. Two other experiments involving a 2% increase of the solar constant and the increase of the cirrus emissivity show the same behavior as that of CO_2 doubling, although the magnitude of the sensitivity varies somewhat.

To summarize the foregoing discussion and to place the cloud–radiation sensitivity into proper perspective, Fig. 4 is a flow diagram illustrating various interactions and feedbacks due to positive radiative forcings (doubling of CO_2, 2% increase in the solar constant, and increase of the cirrus emissivity, as described previously). Increasing the surface temperature caused by a positive radiative forcing will lead to the increase of surface evaporation. This in turn will generate additional water vapor fluxes from the surface to the atmosphere. The subsequent latent heat release will be a positive feedback for atmospheric heating. Moreover, additional water vapor in the atmosphere will also enhance the IR greenhouse effect and produce larger downward IR fluxes, leading to a further increase of surface temperature. This process again is a positive feedback with respect to surface heating. On the other hand, according to our numerical experiments more clouds are also allowed to form in the low level, as a result of which the probability of middle and high clouds being formed is reduced. The solar albedo effect will be predominant in the case of the low cloud cover increase. Furthermore, the reduction of the high cloud cover will decrease the IR greenhouse effect. This, in effect, will enhance the solar albedo effect. Although

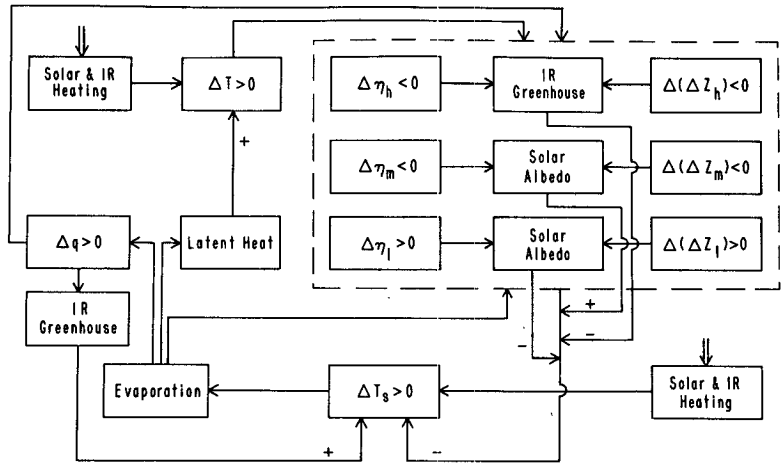

FIG. 4. A flow chart for interactions and feedbacks due to a positive radiative forcing. The plus and minus signs represent positive and negative feedbacks.

the middle cloud cover decrease will reduce the solar albedo effect and hence is a positive feedback in the sensitivity of temperature increases, the net result due to all clouds as illustrated in the present experiment is a negative feedback.

In the present study, cirrus clouds are assumed to be nonblack with emissivities of either 0.47 or 0.62. The nonblack cirrus will not significantly alter the solar flux available to the surface but will increase the downward IR flux due to its emission. As a result, the persistence of optically thin high clouds will exert a heating effect below the cloud. In their pioneering work on the one-dimensional radiative–convective model, Manabe and Wetherald (1967) showed that the greenhouse effect of high clouds increases with increasing blackness. It is noted that they assumed an albedo value for high clouds regardless of their blackness. Increasing cirrus emissivity will result in an increase of the solar albedo value (Ou and Liou, 1984). Consequently, the competition between IR emissivity and solar albedo will lead to a quantitative determination of the greenhouse effect of cirrus clouds. In any event, it suffices to point out that the assumed IR emissivity and the associated solar albedo value are of paramount importance in climatic sensitivity experiments involving clouds.

With respect to cloud thickness variations and temperature perturbations, we find that the feedback sign follows the cloud cover case. That is, as a result of temperature increases, increase and decrease of low and high cloud thicknesses, respectively, will lead to a negative feedback, whereas decrease of the middle cloud thickness will introduce a positive feedback. However, because the thickness of the middle cloud reduces more significantly than those of low and high clouds, the net result when it is coupled with cloud cover variations is a positive temperature feedback in the present cloud–radiation interactive program.

One final note may be in order. In our radiative forcing experiments, we were unable to generate significant changes in the cloud height to examine its effects on temperature perturbations. This is owing to the fact that temperature increases in the aforementioned experiments were relatively small to permit noticeable statistical variations of cloud heights and to introduce sufficient interactions of cloud fields and absorbing gases.

6. Conclusions

In this paper we have developed a one-dimensional climate model with interactive cloud formation and radiative transfer programs. In particular, we showed that the model may be described by a set of partial differential equations. By virtue of the K-theory for the turbulence transfer of sensible and latent heat fluxes, the thermodynamic energy equation is shown to be governed by a first-order partial differential equation for temperature and specific humidity. Moreover, with the neglect of evaporation, the water vapor transport equation is expressed in terms of a second-order differential equation in specific humidity. In addition, the vertical water vapor flux, which is directly proportional to the vertical velocity, is also expressed in the form of a first-order differential equation. To have an effective cloud formation and radiative transfer interaction, we have designed a cloud compaction scheme based on statistical and stochastic analyses to evaluate cloud covers, thicknesses, heights and positions for high, middle and low clouds. Having appropriate boundary conditions defined, including the requirement for the surface energy balance, the layer formation of clouds and the continuity of water vapor fluxes, we illustrated that the system of governing equations may be solved by finite-difference and iterative numerical schemes.

Perturbation experiments were carried out to investigate the effects of interactive cloud formation on

temperature increases due to positive radiative forcings such as doubling of CO_2, a 2% increase of the solar constant, and the increase of the cirrus IR emissivity. Prior to perturbation experiments, reasonably accurate temperature and humidity profiles for mean annual conditions were obtained in reference to available climatological data. Principal findings from the model experiments are that overall the interactive cloud formation and radiative transfer program in positive radiative forcing experiments generates a negative feedback in reference to the fixed cloud program. That is, the sensitivity of temperature increases is reduced. Low and high cloud formations lead to negative feedbacks as a result of the increased low cloud cover and thickness and decreased high cloud cover and thickness. The former strengthens the solar albedo effects, whereas the latter weakens the IR greenhouse effects. On the other hand, the middle cloud formation exhibits a positive feedback because of the reduction in cloud cover and thickness. Further, cloud cover and thickness variations in a positive radiative forcing experiment produce the same sign of feedback, although the degree of influence varies slightly. Finally, it should be pointed out that these results are subject to a number of physical assumptions utilized in the numerical analysis, including a fixed threshold relative humidity, an adjustment of the water vapor diffusion coefficient to the mean annual condition, and a prescribed surface albedo value. Nonetheless, it appears physically appropriate to conclude that an interactive cloud formation with radiative transfer coupling in the context of a model setting will lead to a negative feedback in temperature sensitivity analyses.

Acknowledgments. This research was supported by the Division of the Atmospheric Sciences, National Science Foundation under Grant ATM81-09050 and by the Air Force Geophysics Laboratory under contracts F19628-83-K-0015 and F19628-84-K-0040. Sharon Bennett typed and edited the manuscript.

APPENDIX

Finite-Difference Solutions

Let the level number be denoted from 1 to J and the layer number 1½ to J-½ (see Fig. A1). The water vapor–cloud interactive program is solved first by rewriting Eq. (4.3) in the following finite-difference form:

$$\ln f_{j+1} - \ln f_j = \frac{C_p}{L}\frac{1}{q_{s,j+1/2}(1-\eta_{j+1/2})} \times \left(\frac{\partial T}{\partial z} + \gamma_d\right)_{j+1/2}(z_{j+1} - z_j), \quad j = 1, 2, \cdots, J. \quad \text{(A1)}$$

Upon successive substitutions, the summation form in terms of f_2 consistent with the boundary conditions may be obtained so that

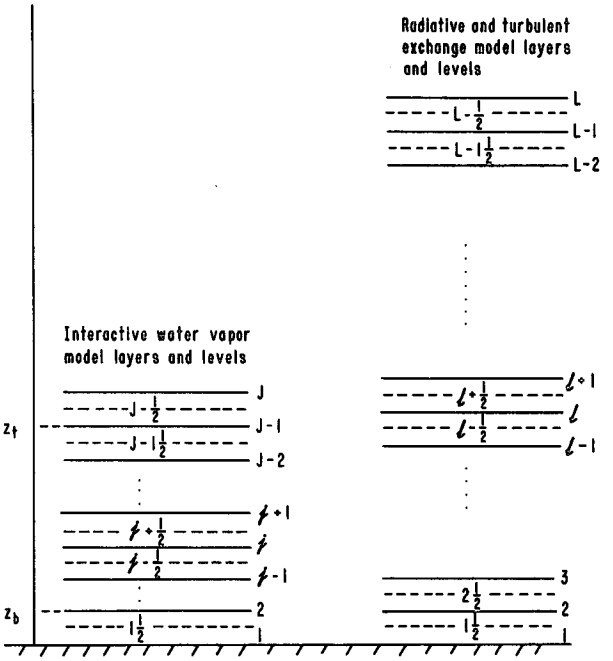

FIG. A1. Level and layer structure for the computations of radiative and turbulent and water vapor fluxes.

$$\ln\frac{f_j}{f_2} = \ln\bar{f}_j = \frac{C_p}{L}\sum_{n=2}^{j-1}\frac{1}{q_{s,n+1/2}(1-\eta_{n+1/2})} \times \left(\frac{\partial T}{\partial z} + \gamma_d\right)_{n+1/2}(z_{n+1} - z_n), \quad j \geq 3. \quad \text{(A2)}$$

By defining $\bar{f}_j = f_j/f_2$, we have nondimensionalized the water vapor flux. Moreover, Eq. (4.12) may be rewritten in the following finite-difference form

$$\bar{f}_2 = -H_L\Big[\sum_{j=2}^{J-2}\eta_{j+1/2}(\bar{f}_{j+1} - \bar{f}_j)\Big]^{-1}. \quad \text{(A3)}$$

Thus, $\bar{f}_2 = 1$ is now the modified boundary condition for Eq. (A2).

The finite-difference form for Eq. (4.2) may be expressed by

$$\left[b_j\left(\frac{q_{j+1/2} - q_{j-1/2}}{z_{j+1/2} - z_{j-1/2}}\right) - b_{j-1}\left(\frac{q_{j-1/2} - q_{j-1^1/_2}}{z_{j-1/2} - z_{j-1^1/_2}}\right)\right]\Big/ (z_j - z_{j-1}) = -H_L\tilde{P}(z_{j-1/2}), \quad (J-1) \geq j \geq 3 \quad \text{(A4)}$$

where

$$\tilde{P}(z_{j-1/2}) = \frac{\eta d\bar{f}/dz}{\int_{z_b}^{z_t}\eta(d\bar{f}/dz)dz} = -\frac{\eta_{j-1/2}f_2(\bar{f}_j - \bar{f}_{j-1})}{H_L(z_j - z_{j-1})}. \quad \text{(A5)}$$

Here we note that $\tilde{P}(z)$ denotes a probability distribution function, which is very similar to the latent heat release distribution function proposed by Kuo (1974) and Anthes (1977) in their cumulus convection mod-

eling. The boundary conditions specified in Eqs. (4.10) and (4.11) may now apply to $q_{1\,1/2}$ and $q_{J-1/2}$ denoted in Eqs. (A4) and (A5). Numerically, for a given $T_j^{(0)}$, we first compute $\bar{f}_j^{(n)}$ from Eq. (A2), and subsequently $\eta_j^{(n)}$ from Eq. (4.4). Then $q_j^{(n)}$ may be evaluated from Eq. (A4), where $n\,(=1, 2, \cdots, N)$ denotes the number of iterations for the convergence of $\bar{f}_j^{(N)}, \eta_j^{(N)}$ and $q_j^{(N)}$.

Next, we couple the water vapor–cloud program with the thermodynamic equation for the solution of the temperature field iteratively. Equation (4.1) is a first-order differential equation in temperature with a nonlinear term contained inside the height integral. We have assumed an initial temperature denoted as $T^{(0)}$. Having new values of $\bar{f}^{(N)}$, $\eta^{(N)}$ and $q^{(N)}$, we proceed to solve a new temperature $T^{(1)}$ based on the following equation:

$$\int_0^\infty \sigma[T^{(1)}(z')]^4 K(|z - z'|)dz' = c(z). \qquad \text{(A6)}$$

We then define a parameter such that

$$\chi^{(m)}(z) = \sigma[T^{(m)}(z)]^4 - \sigma[T^{(1)}(z)]^4, \quad m = 2, 3, \cdots, M \qquad \text{(A7)}$$

where χ so defined (Liou and Ou, 1983) represents the deviation of the desirable Planck flux in reference to the radiative equilibrium Planck flux denoted in Eq. (A6). It follows that Eq. (4.1) may be expressed in the form

$$a(z)\frac{\partial T^{(m)}}{\partial z} + b(z)\frac{\partial q^{(N)}}{\partial z} + \int_0^\infty \chi^{(m)}(z')K(|z - z'|)dz' = 0. \qquad \text{(A8)}$$

In finite difference forms we write

$$a_l\frac{T_{l+1/2}^{(m)} - T_{l-1/2}^{(m)}}{z_{l+1/2} - z_{l-1/2}} + b_l\frac{q_{l+1/2}^{(N)} - q_{l-1/2}^{(N)}}{z_{l+1/2} - z_{l-1/2}} + \chi_1{}^{(m)}K_{l1} + \sum_{i=1}^{L-1}\chi_{i+1/2}^{(m)}K_{li} = g_l[\chi^{(m)}] = 0, \qquad \text{(A9)}$$

where subscript l denotes the level at which the temperature is computed. The third term on the left represents the surface contribution ($l = 1$) and we have introduced a function $g(\chi)$ for the purpose of performing successive iterations where

$$\chi^{(m)} = \begin{bmatrix} \chi_1 \\ \chi_{1^1/_2} \\ \chi_{2^1/_2} \\ \vdots \\ \chi_{L-1/2} \end{bmatrix}^{(m)}. \qquad \text{(A10)}$$

Also, from Eq. (A9) we may derive the slope for the function g in the form

$$\left(\frac{\partial g_l}{\partial \chi_i}\right)^{(m)} = K_{li} + \frac{a_l}{z_{l+1/2} - z_{l-1/2}} \times \left[\left(\frac{\partial T_{l+1/2}}{\partial \chi_i}\right)^{(m)}\delta_{l+1/2,i} + \left(\frac{\partial T_{l-1/2}}{\partial \chi_i}\right)^{(m)}\delta_{l-1/2,i}\right], \quad i = 1, \ 1\tfrac{1}{2}, \ 2\tfrac{1}{2}, \cdots, L - \tfrac{1}{2} \qquad \text{(A11)}$$

where δ is a delta function and note that when $i = 1$, $l - 1/2$ is set to be 1. Moreover, from Eq. (A7) we obtain

$$\left(\frac{\partial \chi_i}{\partial \chi_i}\right)^{(m)} = 1 = 4\sigma[T_i^{(m)}]^3\left(\frac{\partial T_i}{\partial \chi_i}\right)^{(m)}. \qquad \text{(A12)}$$

This allows us to compute $(\partial T_i/\partial \chi_i)$ at the mth iteration step and at the ith level. Finally, by means of the Newton-Raphson Method (Hildebrand, 1956) we may expand the function g in the form

$$g_l[\chi^{(m)}] + \sum_{i=1}^{L}\left(\frac{\partial g_l}{\partial \chi_i}\right)^{(m)}[\chi_i{}^{(m+1)} - \chi_i{}^{(m)}] = 0, \quad l = 1, 2, \cdots, L \qquad \text{(A13)}$$

Since g_l and $\partial g_l/\partial \chi_i$ have been computed via Eqs. (A9) and (A11), $\chi_i{}^{(m+1)}$ may then be solved from Eq. (A13) and $T_i^{(m+1)}$ can subsequently be evaluated from Eq. (A7). The present iterative technique is extremely efficient. Normally, four to five iterations ($M = 4, 5$) are sufficient to converge the temperature solution within about 0.1%. With the new temperature $T_i^{(M)}$, we then go back to the water vapor–cloud program to get the new specific humidity $q_j^{(2N)}$, cloud cover $\eta_j^{(2N)}$ and water vapor flux $\bar{f}_j^{(2N)}$. Iterations are then carried out until four variables are all converged to within 0.1% accuracy.

REFERENCES

Anthes, R. A., 1977: A cumulus parameterization scheme utilizing a one-dimensional cloud model. *Mon. Wea. Rev.*, **105,** 270–286.

Budyko, M. I., 1982: *The Earth's Climate: Past and Future.* Academic Press, 307 pp.

Deardorff, J. W., 1972: Theoretical expression for the counter-gradient vertical heat flux. *J. Geophys. Res.*, **77,** 5900–5904.

Dutton, J. A., 1976: *The Ceaseless Wind.* McGraw-Hill, 579 pp.

Geleyn, J. F., 1981: Some diagnostics of the cloud/radiation interaction in ECMWF forecast model. *Workshop on Radiation and Cloud-Radiation Interaction in Numerical Modeling,* 135–162. [Available from European Centre for Medium Range Weather Forecasts.]

Hansen, J., D. Johnson, A. Lacis, S. Lebedeff, P. Lee, D. Rind and G. Russell, 1981: Climate impact of increasing atmospheric carbon dioxide. *Science,* **213,** 957–966.

——, G. Russell, D. Rind, P. Stone, A. Lacis, S. Lebedeff, R. Ruedy and L. Travis, 1983: Efficient three-dimensional global models for climate studies: Models I and II. *Mon. Wea. Rev.*, **111,** 609–662.

Hildebrand, F. B., 1956: *Introduction to Numerical Analysis.* McGraw-Hill, 511 pp.

Hummel, J. R., and W. R. Kuhn, 1981: An atmospheric radiative-convective model with interactive water vapor transport and cloud development. *Tellus,* **33,** 372–381.

Kuo, H. L., 1974: Further studies of the parameterization of the influence of cumulus convection on large-scale flow. *J. Atmos. Sci.*, **31**, 1232–1240.

Liou, K. N., and S. S. Ou, 1983: Theory of equilibrium temperature in radiative–turbulent atmospheres. *J. Atmos. Sci.*, **40**, 215–229.

——, and Q. Zheng, 1984: A numerical experiment on the interactions of radiation, clouds and dynamic processes in a general circulation model. *J. Atmos. Sci.*, **41**, 1513–1535.

London, J., 1957: A study of the atmospheric heat balance. New York University, Final Rep. Contract AF19(122)-166, 99 pp.

Manabe, S., and R. T. Wetherald, 1967: Thermal equilibrium of the atmosphere with a given distribution of relative humidity. *J. Atmos. Sci.*, **24**, 241–259.

Oort, A. H., and E. M. Rasmusson, 1971: *Atmospheric Circulation Statistics.* NOAA Prof. Paper 5, U.S. Department of Commerce, 323 pp. (DOCC 55.25:5).

Ou, S. S., and K. N. Liou, 1984: A two-dimensional radiative–turbulence climate model. I: Sensitivity to cirrus radiative properties. *J. Atmos. Sci.*, **41**, 2289–2309.

Ramanathan, F., and J. A. Coakley, Jr., 1978: Climate modeling through radiative-convective models. *Rev. Geophys. Space. Phys.*, **16**, 465–489.

Reed, R. J., and K. E. German, 1965: A contribution to the problem of stratospheric diffusion by large-scale mixing. *Mon. Wea. Rev.*, **93**, 313–321.

Sasamori, T., 1975: A statistical model for stationary atmospheric cloudiness, liquid water content, and rate of precipitation. *Mon. Wea. Rev.*, **103**, 1037–1049.

Sellers, W. D., 1965: *Physical Climatology.* The University of Chicago Press, 272 pp.

Sundqvist, H., 1978: A parameterization scheme for non-convective condensation including prediction of cloud water content. *Quart. J. Roy. Meteor. Soc.*, **104**, 677–690.

Washington, W. M., and G. A. Meehl, 1984: Seasonal cycle experiment on the climate sensitivity due to a doubling of CO_2 with an atmospheric general circulation model coupled to a simple mixed-layer ocean model. *J. Geophys. Res.*, **89**, 9475–9503.

Wetherald, R. T., and S. Manabe, 1980: Cloud cover and climate sensitivity. *J. Atmos. Sci.*, **37**, 1485–1510.